

**Interatomic Coulombic decay in a He dimer: *Ab initio* potential-energy curves and decay widths**Přemysl Kolorenč,<sup>1</sup> Nikolai V. Kryzhevoi,<sup>2,\*</sup> Nicolas Sisourat,<sup>2</sup> and Lorenz S. Cederbaum<sup>2</sup><sup>1</sup>*Faculty of Mathematics and Physics, Institute of Theoretical Physics, Charles University in Prague, V Holešovičkách 2, 180 00 Prague, Czech Republic*<sup>2</sup>*Theoretische Chemie, Universität Heidelberg, Im Neuenheimer Feld 229, D-69120 Heidelberg, Germany*

(Received 7 June 2010; published 28 July 2010)

The energy gained by either of the two helium atoms in a helium dimer through simultaneous ionization and excitation can be efficiently transferred to the other helium atom, which then ionizes. The respective relaxation process called interatomic Coulombic decay (ICD) is the subject of the present paper. Specifically, we are interested in ICD of the lowest of the ionized excited states, namely, the  $\text{He}^+(n=2)\text{He}$  states, for which we calculated the relevant potential-energy curves and the interatomic decay widths. The full-configuration interaction method was used to obtain the potential-energy curves. The decay widths were computed by utilizing the Fano ansatz, Green's-function methods, and the Stieltjes imaging technique. The behavior of the decay widths with the interatomic distance is examined and is elucidated, whereby special emphasis is given to the asymptotically large interatomic separations. Our calculations show that the electronic ICD processes dominate over the radiative decay mechanisms over a wide range of interatomic distances. The ICD in the helium dimer has recently been measured by Havermeier *et al.* [*Phys. Rev. Lett.* **104**, 133401 (2010)]. The impact of nuclear dynamics on the ICD process is extremely important and is discussed by Sisourat *et al.* [*Nat. Phys.* **6**, 508 (2010)] based on the *ab initio* data computed in the present paper.

DOI: [10.1103/PhysRevA.82.013422](https://doi.org/10.1103/PhysRevA.82.013422)

PACS number(s): 33.80.Eh, 31.15.ag, 31.50.Df

**I. INTRODUCTION**

A helium atom is the next simplest atom after hydrogen. Its structure consists of a completed shell that comprises two electrons, which orbit around the nucleus. These electrons are very tightly bound such that, in order to remove either of them from the system, energy of 24.6 eV is needed. Even stronger energy is required to excite or to ionize the remaining electron. For instance, the excitation of a helium ion to the level with the principal quantum number  $n$  of 2 uses 40.8 eV, to the level with  $n = 3$ , 48.3 eV, and so on, until ionization of the last electron occurs at the energy of 54.4 eV [1].

A simultaneously ionized and excited isolated helium atom decays radiatively by emitting a single photon with an exception for the metastable  $2s$  state, where double photon emission is the most probable mode of the radiative decay [2]. It is worthwhile to note that the energy released in these deexcitation processes greatly exceeds the ionization threshold of any neutral system in nature. Thus, at the presence of any system in the neighborhood of an ionized excited helium atom, the latter has the possibility to get rid of its excess energy through electronic interatomic Coulombic decay (ICD) [3]. The feasibility of ICD of an ionized excited helium atom was recently demonstrated by experimentalists from the Dörner group in Frankfurt in the extreme case of a helium dimer [4].

The peculiarity of the helium dimer consists of its weakly bound character. With a binding energy of only 1.1 mK [5]  $\text{He}_2$  is the weakest bound cluster. The wave function of its ground state is so delocalized that the mean distance between the two helium atoms constitutes enormous 52 Å [5], although the minimum of the respective potential-energy curve is at 2.97 Å only (see, for example, Refs. [6–8]). Thus, a He dimer represents a unique system, which provides an excellent

opportunity for studying the ultralong-range transfer of energy during ICD between an ionized excited helium atom and its neutral partner.

By utilizing cold target recoil ion momentum spectroscopy [9], Havermeier and co-workers investigated the fragmentation dynamics of a helium dimer which follows simultaneous ionization and excitation of one of its constituent atoms to energy levels characterized by different principal quantum numbers  $n$  [4]. A spectacularly long-range energy transfer was revealed in these experiments, which provided evidence that ICD can be operative when the separation between helium atoms is significantly larger than their atomic radii. The fact, which also merits particular attention, was the first observation of a vibrational structure in the ICD spectra that points to the paramount role of the nuclear motion in the ICD process.

In the present paper, we address ICD of the lowest-energy states in the sequence of the ionized excited states of a helium atom in  $\text{He}_2$ , namely, the  $\text{He}^+(n=2)\text{He}$  ones. The potential-energy curves of these states as well as of the final ICD states  $\text{He}^+(1s)\text{He}^+(1s)$ , which describe two helium ions in their ground electronic states have been computed by using the *ab initio* full-configuration interaction (FCI) method. We have also performed *ab initio* calculations of the ICD widths in order to compare the performance of the respective electronic decay with that of the competitive radiative decay. These calculations have been done by utilizing a combination of the Fano ansatz, Green's-function methods, and the Stieltjes imaging technique [10,11].

It should be emphasized that there exist remarkable differences between the ICD considered in this paper and the ICD processes reported earlier. Note that ICD was originally predicted and then predominantly sought as a possible electronic decay of inner valence vacancies in weakly bound systems (see, for example, Refs. [3,12–19]). In addition, the feasibility of ICD in a core-level regime was demonstrated as well by examples of several systems [20–22]. In a helium

\*nikolai.kryzhevoi@pci.uni-heidelberg.de

dimer, neither the core nor an inner valence shell is present. Here, outer valence ionized states undergo ICD. Moreover, we deal with interatomic Coulombic decay of secondary satellite states in the photoelectron spectrum rather than with ICD of the main states. Since ICD of satellite states has not yet been studied theoretically, ICD in the helium dimer, as a function of the interatomic distance, deserves close inspection in this paper. We pay particular attention to distinct behaviors of ICD widths related to different electronic states at asymptotically large interatomic separations and give explanations for these behaviors.

Finally, we mention that the *ab initio* results presented in this paper were used as input data for studying nuclear dynamics during the ICD processes that occur in  $\text{He}_2$ . The results of these computations are reported by Sisourat *et al.* [23].

## II. COMPUTATIONAL DETAILS

The total energies of the initial (decaying)  $\text{He}^+(n=2)\text{He}$  and the final  $\text{He}^+(1s)\text{He}^+(1s)$  states at internuclear distances from 1 to 50 Å were computed by means of the FCI method by using the GAMESS-US quantum chemistry package [24]. In choosing the basis set, we looked for a compromise between the accuracy of computations and the numerical efforts required. The ground and the first excited states of the isolated helium cation with their energies of  $-2.0$  and  $-0.5 E_H$ , respectively, as predicted by the nonrelativistic theory, were used as the reference states. By employing a basis set of sextuple-zeta quality, we obtained  $-1.999\,993\,37 E_H$  for the ground-state energy of  $\text{He}^+$  and  $-0.499\,997\,56$  and  $-0.499\,996\,96 E_H$  for the energies of the excited  $\text{He}^+(2p)$  and  $\text{He}^+(2s)$  states, respectively. The basis set of our choice was composed of the Dunning cc-pV6Z basis set [25], where all  $f$ ,  $g$ , and  $h$  functions were deleted. The influence of these functions on the energies of the reference states was found to be negligible. In contrast, two  $s$  ( $\alpha_s = 0.044\,73, 0.0146$ ) and two  $p$  ( $\alpha_p = 0.128, 0.0424$ ) diffuse functions and especially two  $s$  ( $\alpha_s = 0.245\,645, 0.098\,496$ ) and three  $p$  ( $\alpha_p = 0.430\,082, 0.169\,341, 0.089\,894$ ) Gaussian continuumlike functions of the Kaufmann-Baumeister-Jungen (KJB) type [26] were found to significantly contribute to the accurate description of the reference states and were added to the basis set. The computations on the He dimer were performed by placing the described basis set on each helium atom. All of the resulting 120 molecular orbitals were included in the active space in the FCI computations.

Interatomic decay rates for the six decaying states of the  $\text{He}^+(n=2)\text{He}$  type have been calculated by utilizing a combination of the Fano ansatz, the extended second-order algebraic diagrammatic construction scheme for the one-particle Green's function [1p-GF/ADC(2)x], and the Stieltjes imaging method. At this level of theory, the many-body electronic wave functions are expanded in terms of one-hole (1h) and two-hole one-particle (2h1p) configurations derived from the closed-shell Hartree-Fock (HF) ground state of the neutral dimer. The present application implies the use of the Fano-ADC-Stieltjes method adapted for symmetric systems [11]. The basic concept of the inversion symmetry-adapted Fano-ADC-Stieltjes method is the partitioning of the ADC

configuration space, namely, its 2h1p part, to one-site and two-site parts. The initial (discrete) state of the decay process is then expanded in the subspace of the one-site configurations, while the final states are represented as linear combinations of the two-site configurations. The present problem fundamentally differs from previous applications of the method in that the decaying  $\text{He}^+(n=2)\text{He}$  states are, themselves, of the 2h1p character, like the final states of the decay  $\text{He}^+(1s)\text{He}^+(1s)$ . It is easily verified, though, that the approach can also readily be applied to the calculation of the interatomic decay rate of a one-site 2h1p-like satellite state, by assuming that the state of interest is well defined in the satellite spectrum. The accuracy of the calculated decay widths is expected to be lower due to the lower quality of the ADC representation of satellite states compared to the main space. However, the method still goes beyond the first-order perturbation-theoretical expression for the interatomic decay width, since the correlation between the considered 2h1p configurations accounts for higher-order decay pathways.

Since there are only two molecular orbitals occupied in the neutral  $\text{He}_2$ ,  $1\sigma_g$  and  $1\sigma_u$ , the ADC expansion is considerably simplified. In the relevant doublet spin multiplicity, four types of (spin adapted) 2h1p configurations are available for a singly ionized helium dimer— $|\sigma_g\sigma_u\mathbf{k}^\dagger\rangle_t$ ,  $|\sigma_g\sigma_u\mathbf{k}^\dagger\rangle_s$ ,  $|\sigma_g\sigma_g\mathbf{k}^\dagger\rangle_s$ , and  $|\sigma_u\sigma_u\mathbf{k}^\dagger\rangle_s$ . Here,  $\sigma_{g(u)}$  denotes the annihilation of an electron in one of the occupied orbitals, while  $\mathbf{k}^\dagger$  corresponds to the creation of an electron in a virtual (possibly continuum) orbital. Subscripts  $t$  and  $s$  refer to the configuration, which is derived from triplet and singlet 2h states, respectively. While the  $|\sigma_g\sigma_u\mathbf{k}^\dagger\rangle_t$  configurations belong directly in the two-site class and  $|\sigma_g\sigma_u\mathbf{k}^\dagger\rangle_s$  belongs in the one-site class, in the other two types of configurations, the one- and two-site states are mixed. These configurations have to be adapted via diagonalization of the corresponding  $2 \times 2$  Hamiltonian matrix (for fixed virtual orbital  $\mathbf{k}$ ). The higher-lying eigenstate belongs to the one-site states and enters the initial-state expansion, while the lower-lying eigenstate contributes to the final-state expansion.

We remark that the 1h configurations  $|\sigma_g\rangle$  and  $|\sigma_u\rangle$  are excluded from both the initial- and the final-state expansions. The effect of inclusion of the 1h configurations in the final-state expansions was negligible due to their weak correlation with two-site 2h1p-like states. On the other hand, correlation of the  $|\sigma_{g(u)}\rangle$  configurations with the  ${}^2\Sigma_{g(u)}$  initial states with the  $\text{He}^+(2s)\text{He}$  asymptote is rather large. At the present level of theory, however, consequential correlation imbalance between the initial and the final states is induced, which leads to qualitatively wrong dependence of the interatomic decay rate on the interatomic distance upon inclusion of the  $|\sigma_{g(u)}\rangle$  configurations into the initial-state expansion. To restore the balance, certain 3h2p configurations are needed in the final-state expansions, which are not available in the 1p-GF/ADC(2)x approximation scheme. Therefore, the 1h configurations have to be excluded from the ADC expansion, despite the lowered quality of representation of certain initial states.

The calculations have been performed by using the MOLCAS quantum chemistry package [27] and the Fano-ADC-Stieltjes code of Averbukh and Cederbaum [11]. On the atomic centers, the cc-pV6Z basis of Dunning [25] was used, augmented by  $[9s, 9p, 9d]$  continuumlike Gaussian functions of the KJB type.

In addition,  $[5s, 5p, 5d]$  KJB-type basis sets were used at three ghost centers located between the two He atoms.

### III. RESULTS AND DISCUSSION

#### A. Potential-energy curves

Figure 1 shows potential-energy curves of the initial and final states of the ICD processes addressed in this paper, together with the ground state of the neutral He dimer. The latter was not calculated in the present paper but was taken from Ref. [6]. Its remarkable properties are well described in the literature [5,7,8]. Here, we only mention that the respective potential-energy curve exhibits an extremely shallow minimum of the depth of 1 meV at 2.97 Å and only supports a single bound vibrational state.

Doubly ionized states of He<sub>2</sub> have attracted considerable attention as well [28–31]. Particular emphasis has been paid to the ground  $^1\Sigma_g^+$  state of He<sub>2</sub><sup>2+</sup>, which is one of the two possible final ICD states. The respective potential-energy curve shows interesting behavior at short internuclear distances. Exchange interactions and electron-nuclear attraction overcome the nuclear repulsion there, which gives rise to a local minimum at 0.75 Å and to a local maximum at 1.14 Å. The latter is seen in Fig. 1. It must be said that such short internuclear separations are irrelevant for ICD, which is operative at larger internuclear distances, where the  $^1\Sigma_g^+$  curve is repulsive. The second final ICD state  $^3\Sigma_u^+$  is repulsive over all internuclear distances.

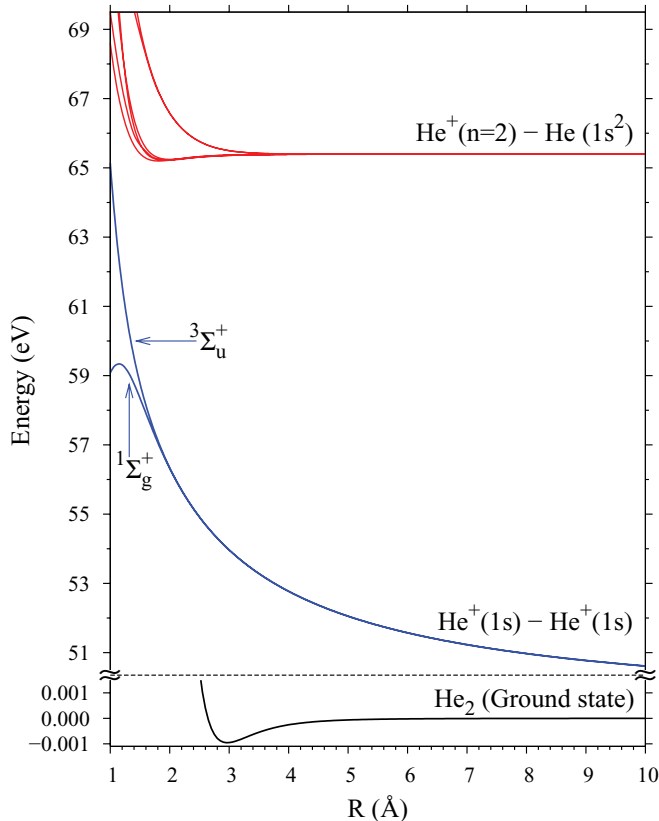


FIG. 1. (Color online) Electronic states involved in the ICD processes. Apart from the ground state of He<sub>2</sub> taken from Ref. [6], all other states were calculated by using the FCI method.

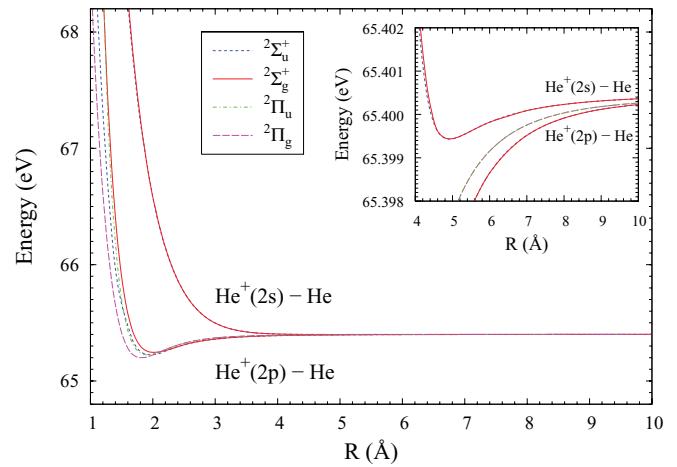


FIG. 2. (Color online) Calculated potential-energy curves of the He<sup>+</sup>( $n = 2$ )He states. An expanded energy region around  $R = 5$  Å is shown in the inset.

In contrast to the ground state of the neutral He dimer and to the final ICD states, the decaying He<sup>+</sup>( $n = 2$ )He states so far have not received any consideration. A closer view of these ionized excited states is shown in Fig. 2. Altogether, there are six states, which describe ionization and excitation to a state with  $n = 2$  of either helium atom in the helium dimer. These are two doubly degenerate  $^2\Pi_{g,u}$  states and four  $^2\Sigma_{g,u}^+$  states. Excitations to the  $2p_{x,y}$  orbitals, which are directed perpendicular to the molecular axis give rise to the  $\Pi$  states, whereas excitations to the on-axis  $2p_z$  orbital and to the  $2s$  one form the  $\Sigma$  states. Together with the molecular electronic terms nomenclature, we also use a notation where electronic states are distinguished according to the orbital to which an electron is excited:  $2p$  or  $2s$ . We note, however, that, at internuclear distances shorter than about 5 Å, the  $2p_z$  and  $2s$  orbitals are strongly mixed and, therefore, the He<sup>+</sup>( $2s$ )He and He<sup>+</sup>( $2p$ )He labels are not strictly valid.

Each of the potential-energy curves He<sup>+</sup>( $2p$ )He has a pronounced minimum, which is found at shorter internuclear distances compared to the minimum at the potential-energy curve of the neutral helium dimer. The minimum of the  $^2\Pi_g$  state, which is the ground state of the He<sup>+</sup>( $n = 2$ )He system is at 1.8 Å. The other three states,  $^2\Pi_u$ ,  $^2\Sigma_g^+$ , and  $^2\Sigma_u^+$  have their minima at 1.9, 2.0, and 1.96 Å, respectively. In contrast, the minima of the He<sup>+</sup>( $2s$ )He curves are very shallow, each of a depth of 1.0 meV, and are found at 4.9 Å (see the inset in Fig. 2).

#### B. Interatomic decay widths

Figure 3 shows the calculated total interatomic decay widths for the He<sup>+</sup>( $n = 2$ )He → He<sup>+</sup>( $1s$ )He<sup>+</sup>( $1s$ ) + e<sup>-</sup> transitions. Both the molecular electronic terms nomenclature and the atomic-orbital notation are used to fully distinguish between the six different decaying states. From the point of view of the expansion of the corresponding ADC eigenvectors, the He<sup>+</sup>( $2p_z$ )He and He<sup>+</sup>( $2s$ )He characters of the  $^2\Sigma_{g(u)}$  decaying states cannot be unambiguously identified for internuclear distances shorter than 5 Å. However, the remarkable difference in

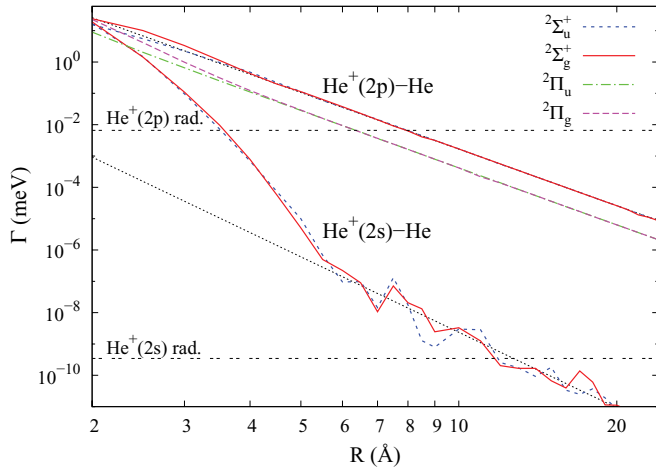


FIG. 3. (Color online) Total ICD widths of the six metastable states  $\text{He}^+(n=2)\text{He}$ . The dotted lines show the asymptotic trends  $R^{-6}$  and  $R^{-8}$  for the initial states of the  $\text{He}^+(2p)\text{He}$  and  $\text{He}^+(2s)\text{He}$  characters, respectively. Numerical instability of the ICD width for the  $\text{He}^+(2s)\text{He}$  states is manifested for  $R > 6 \text{ \AA}$ . Its origin is discussed in the text. Horizontal double-dashed lines show the respective radiative decay widths for the  $\text{He}^+(2p)$  ( $\tau_{\text{rad}} = 99.7 \text{ ps}$ , [32]) and  $\text{He}^+(2s)$  ( $\tau_{\text{rad}} = 1.9 \text{ ms}$ , [33]) atomic ions. Note the double logarithmic scale of the plot.

the qualitative behavior of the ICD widths clearly distinguishes between the two types of initial states.

We observe that the ICD widths for all four initial states characterized by the helium ion with electrons excited to the  $2p$  orbital exhibit the  $R^{-6}$  dependence on the internuclear distance  $R$ , expected for the dipole-allowed ICD transitions [16,34]. In this case, the transfer of the excess energy from the initially ionized and excited atom to the neutral one can be understood as being mediated via a single virtual photon. Only a slight deviation from the  $R^{-6}$  trend can be seen for  $R < 4 \text{ \AA}$ . The dipole-dipole interaction character of the interatomic decay of these metastable states is further confirmed by the dependence of the decay width on the orientation of the  $2p$  orbital occupied in the initial state. The ratio between the total widths for an electron in the  $2p$  orbital oriented along and perpendicular to the molecular axis is 4 for interatomic distances larger than  $R = 5 \text{ \AA}$ . This factor is in precise agreement with the analysis of the dependence of the interatomic decay rates on the symmetry of initial excitation [35]. It has been shown that this ratio can be explained by the dependence of the interaction energy of two classical dipoles on their mutual orientation.

Strikingly different behavior of the ICD widths is observed for the other two decaying states. The decay widths decrease exponentially for  $R < 6 \text{ \AA}$ , where the widths reach very small magnitude on the order of  $10^{-7} \text{ meV}$ . Only for even larger internuclear distances can an inverse power law be observed. Despite certain numerical instabilities of the present calculations of such small decay widths, the  $R^{-8}$  trend is clearly seen. This behavior clearly marks the corresponding initial states as being characterized by the helium ion with electrons excited to the  $2s$  atomic orbital, since the  $\text{He}^+(2s) \rightarrow \text{He}^+(1s)$  transition is not dipole driven. In fact, in an isolated helium ion, the  $\text{He}^+(2s)$  excited state cannot decay by a single-

photon emission [2]. This breaks the virtual photon-transfer picture of ICD, discussed in the context of the decay of the  $\text{He}^+(2p)\text{He}$  initial states, and makes the orbital overlap effects [16] in the dimer the dominant driving force of the nonradiative interatomic decay process, which results in the exponential dependence of the interatomic decay widths on the internuclear distance.

The question arises whether the observed  $R^{-8}$  behavior can be interpreted in terms of quadrupole-driven transition in analogy with the interatomic decay of  $d$  vacancies for the elements of the periodic table groups 3–12, such as  $\text{BaZn}^+(3d^{-1})$  [16]. The answer is no—this would again correspond to the single-photon transition picture, which is not valid in the present case. Hence, any deviation from the exponential decrease of the decay widths cannot be explained within the first-order Wigner-Weisskopf theory of ICD [36]. The second-order Wigner-Weisskopf expression for the decay width reads

$$\Gamma = 2\pi \left| \sum_i \frac{\langle f | \hat{V} | i \rangle \langle i | \hat{V} | 0 \rangle}{E_0 - E_i} \right|^2 \delta(E_f - E_0), \quad \hat{V} = \sum_{p < q} \frac{e^2}{r_{pq}}, \quad (1)$$

where  $|0\rangle$  is the initial excited singly ionized state,  $|f\rangle$  is the final state of the decay, and  $|i\rangle$ 's are the so-called intermediate states. Equation (1) suggests that, in the second order of perturbation theory (PT), the nonradiative transition can be interpreted as a superposition of decay pathways defined by an intermediate state  $|i\rangle$ , for which the energy conservation is not required. Detailed analysis shows, however, that, even in the second order of PT, the observed  $R^{-8}$  trend cannot be explained, since even the most efficient decay pathways lead only to the  $R^{-10}$  dependence of the interatomic decay width.

It is only the third order of PT, in which we have to analyze all the decay pathways, which involve two intermediate states,  $|i\rangle$  and  $|j\rangle$ , where the origin of the observed  $R^{-8}$  asymptotic behavior of the decay width of the  $\text{He}^+(2s)\text{He}$  state can be revealed. By neglecting the inversion symmetry of the system and by assuming that atom  $A$  is initially ionized and atom  $B$  is initially neutral, one of the relevant decay pathways is

$$\begin{aligned} |(\widetilde{2s}_A)^\dagger(1s_B)^\dagger(1s_B)^\dagger\rangle &\rightarrow |(\widetilde{2p_{z,A}})^\dagger(1s_B)^\dagger(1s_B)^\dagger\rangle \\ &\rightarrow |(1s_A)^\dagger(1s_B)^\dagger(1s_B)^\dagger\rangle \\ &\rightarrow |(1s_A)^\dagger(1s_B)^\dagger\tilde{\mathbf{k}}_B^\dagger\rangle. \end{aligned} \quad (2)$$

The ket vectors represent spin-adapted three-electron wave functions, which are not derived from the HF ground state but from bare nuclei (should not be mistaken for the  $2h1p$  configurations used during the discussion of the ADC scheme). Here, the symbol  $\dagger$  denotes the creation of an electron, and the tilde above the orbital implies an atomic orbital of the  $\text{He}^+$  ion. Hence,  $(1s_B)^\dagger$  corresponds to an electron in the  $1s$  orbital of the neutral atom  $B$ , while  $\tilde{\mathbf{k}}_B^\dagger$  describes an electron in a continuum orbital of the ionized atom  $B$ . We distinguish between the atomic orbitals that correspond to the neutral He and to the  $\text{He}^+$  ion. This means that, for instance, the  $1s_A$  and the  $\widetilde{2s}_A$  orbitals are not mutually orthogonal. Overlap between atomic orbitals on two different atoms is, on the other

hand, neglected, since we only consider large internuclear distances.

The contribution of the decay pathway described by Eq. (2) to the interatomic decay width is represented by the product of three Coulomb integrals, which reads

$$\begin{aligned} & \langle f | \hat{V} | i \rangle \langle i | \hat{V} | j \rangle \langle j | \hat{V} | 0 \rangle \\ & = 2\sqrt{2} \langle 1s_B \widetilde{1s}_B | 1s_B \widetilde{\mathbf{k}}_B \rangle \langle 2p_{z,A} \widetilde{1s}_A | 1s_B 1s_B \rangle \\ & \quad \times \langle 2s_A 2p_{z,A} | 1s_B 1s_B \rangle. \end{aligned} \quad (3)$$

By reading the integrals from right to left, the first integral describes the polarization of the initially ionized atom  $2s_A \rightarrow 2p_{z,A}$ , induced by the presence of the neighboring helium. The middle one corresponds to the  $2p_{z,A} \rightarrow 1s_A$  deexcitation on atom  $A$ . The leftmost integral describes ejection of the ICD electron from atom  $B$ ,  $1s_B \rightarrow \widetilde{\mathbf{k}}_B$ , with simultaneous relaxation  $1s_B \rightarrow \widetilde{1s}_B$ . Expansion in terms of inverse powers of the internuclear distance  $R$  shows that this integral does not depend on  $R$ , since both transitions take place on a single atom, while the other two integrals, which involve both atoms behave asymptotically as  $R^{-2}$ . Hence, contribution to the interatomic decay width, which arises solely from the considered pathway exhibits the sought  $R^{-8}$  behavior, observed in the calculated decay width of  $\text{He}^+(2s)\text{He}$  initial states. The fact that the leading term in the asymptotic expansion appears only in the third order of PT explains the small magnitude of the decay rate in the region where the orbital overlap effects become negligible.

For a complete understanding and a simulation of the ICD electron spectra, not only the total ICD widths are needed, but also partial decay widths are needed. They were calculated as described in Ref. [10]. As shown in Fig. 1, there are only two available decay channels, namely, the  $^1\Sigma_g^+$  and  $^3\Sigma_u^+$  states of  $\text{He}^+(1s)\text{He}^+(1s)$ . Calculated partial decay widths are shown in Fig. 4 for two selected metastable states of  $\text{He}^+(n=2)\text{He}$ . We see that the relaxation of the  $\text{He}^+(2p_z)\text{He}$  state is strongly dominated by the decay into the triplet channel, the triplet to singlet ratio being around 3.5. The same picture also holds for other studied metastable states with the electron excited to the  $2p$  orbital. Excitation of the electron to the  $2s$  orbital leads to different results not only from the point of view of asymptotic behavior, but also concerning the partial widths. As seen in the upper panel of the figure, decay into the singlet channels is, in this case, preferred, but the singlet to triplet ratio varies only around 1.6.

The unsmooth behavior of the total and partial ICD widths seen in Figs. 3 and 4 for the  $\text{He}^+(2s)\text{He}$  states at large  $R$  is partially understood by the very small absolute values of these widths. A more thorough explanation of this behavior lies in the fact that, in the region of the  $R^{-8}$  dependence of  $\Gamma(R)$  ( $R > 6 \text{ \AA}$ ), the coupling matrix elements are dominated by products of three two-electron integrals [see Eq. (3)], which correspond to third-order PT pathways. This leads to the accumulation of relative errors, which arise from the integrals evaluation and diagonalization of the ADC Hamiltonian matrix. In the region of the exponential dependence of the decay width ( $R < 6 \text{ \AA}$ ), on the other hand, the coupling matrix elements are dominated by first-order PT contributions (i.e., a single two-electron integral), and the relative errors, therefore, are smaller.

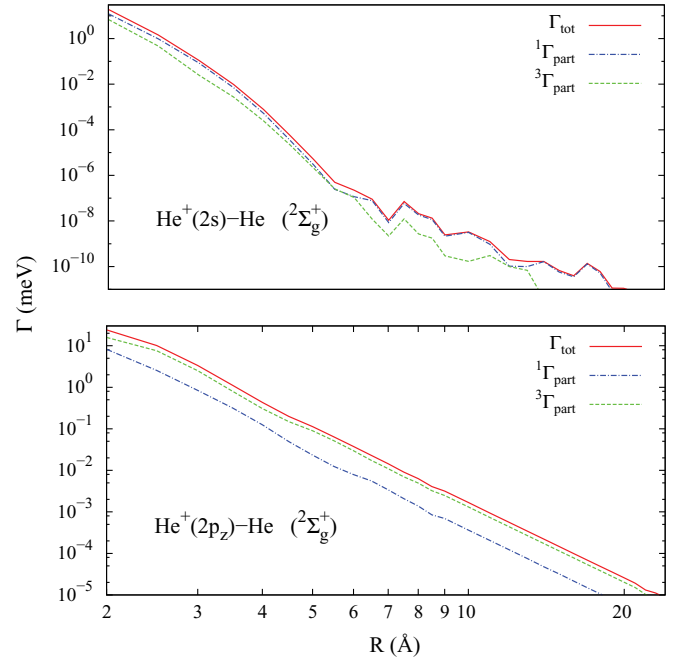


FIG. 4. (Color online) Total (full lines) and partial ICD widths into the singlet (dashed-dotted) and triplet (dashed) channels for two metastable states of the  $^2\Sigma_g^+$  symmetry. The upper panel corresponds to the  $\text{He}^+(2s)\text{He}$  decaying state, while the lower panel corresponds to the  $\text{He}^+(2p_z)\text{He}$  one. Numerical instability of the ICD width for the  $\text{He}^+(2s)\text{He}$  states is manifested for  $R > 6 \text{ \AA}$ . Its origin is discussed in the text.

#### IV. CONCLUSIONS

The present paper comprises the theoretical description of the interatomic Coulombic decay in a helium dimer. Here, we report on the *ab initio* calculations of quantities necessary for the computation of the ICD electron spectrum, namely, the potential-energy curves of the initial and final states of the decay and the interatomic decay widths.

The total energies of the six decaying  $\text{He}^+(n=2)\text{He}$  and the two final  $\text{He}^+(1s)\text{He}^+(1s)$  states were calculated by means of the FCI method, which employs extended basis sets. All  $\text{He}^+(2p)\text{He}$  states exhibit well-defined minima at internuclear distances of 1.8–2.0  $\text{ \AA}$ . In contrast, the minima at the  $\text{He}^+(2s)\text{He}$  curves are much more shallow and are displaced to remarkably larger internuclear distances, namely, to 4.9  $\text{ \AA}$ . Both final ICD states are fully repulsive at the distances relevant to the interatomic decay.

The total and partial interatomic decay widths for the six considered initial states were calculated by employing the inversion symmetry-adapted Fano-ADC-Stieltjes method [11], based on the extended second-order ADC scheme for the one-particle Green's function. The results show that the initial states of the interatomic decay in helium dimer split essentially into two groups according to the symmetry of the second-shell orbital into which the single electron on the ionized helium has been excited. If the electron has been excited into the  $2p$  orbital, the corresponding interatomic decay is driven by a dipole-dipole interaction between the two atoms and falls into the well-analyzed class of ICD processes, which is qualitatively described by the virtual photon-exchange picture.

The dipole-dipole nature of the decay is confirmed particularly by the  $R^{-6}$  dependence of the decay widths on the internuclear distance and by the ratio of the widths, which correspond to states with the  $2p$  orbital oriented along or perpendicular to the molecular axis.

The distinctive feature of the second class of initial states with the excited electron in the  $2s$  orbital of ionized helium is the exponential decrease of the interatomic decay widths with increasing internuclear distance. Such behavior indicates the leading role of orbital overlap effects in the nonradiative decay process. As a result, apart from very small internuclear distances, this class of metastable states exhibits considerably longer lifetimes. At larger internuclear distances, the exponential decrease is superseded by the  $R^{-8}$  asymptotic behavior, which has to be traced down to the third order of PT. The origin of this remarkable difference, as compared to the decaying states characterized by the  $2p$  electron, lies in the fact that the transition of an electron between two  $s$  orbitals in the initially ionized helium cannot be mediated by a single-photon emission. This results in the breakdown of the first-order perturbation-theoretical description and

the virtual photon-transfer picture of the interatomic decay process.

The ICD strongly dominates over the radiative decay for interatomic distances smaller than about  $10 \text{ \AA}$ , whereby ICD in a He dimer is a rather slow process, which takes place in the time scale of a few tens of picoseconds. Thus, a reliable picture of ICD in this system cannot be obtained without taking the motion of the atomic nuclei into account. The corresponding computations have been performed and have been reported in Ref. [23].

#### ACKNOWLEDGMENTS

The authors thank V. Averbukh for providing the Fano-ADC-Stieltjes code. This work has been financially supported by the Deutsche Forschungsgemeinschaft, the Alexander von Humboldt foundation, the European Research Council (ERC Advanced Investigator Grant No. 227597), the Czech Science Foundation (Grant No. GAČR 202/09/0786) and the Ministry of Education, Youth and Sports of Czech Republic (the institutional research Plan No. MSM0021620860).

- 
- [1] Y. Ralchenko, A. E. Kramida, J. Reader, and the NIST ASD team, *NIST Atomic Spectra Database* (version 3.1.5) (National Institute of Standards and Technology, Gaithersburg, MD, 2008).
- [2] J. Shapiro and G. Breit, *Phys. Rev.* **113**, 179 (1959).
- [3] L. S. Cederbaum, J. Zobeley, and F. Tarantelli, *Phys. Rev. Lett.* **79**, 4778 (1997).
- [4] T. Havermeier *et al.*, *Phys. Rev. Lett.* **104**, 133401 (2010).
- [5] R. E. Grisenti, W. Schöllkopf, J. P. Toennies, G. C. Hegerfeldt, T. Köhler, and M. Stoll, *Phys. Rev. Lett.* **85**, 2284 (2000).
- [6] K. T. Tang, J. P. Toennies, and C. L. Yiu, *Phys. Rev. Lett.* **74**, 1546 (1995).
- [7] R. J. Gdanitz, *Mol. Phys.* **99**, 923 (2001).
- [8] T. van Mourik and T. H. Dunning Jr., *J. Chem. Phys.* **111**, 9248 (1999).
- [9] J. Ullrich, R. Moshhammer, A. Dorn, R. Dörner, L. Ph. H. Schmidt, and H. Schmidt-Böcking, *Rep. Prog. Phys.* **66**, 1463 (2003).
- [10] V. Averbukh and L. S. Cederbaum, *J. Chem. Phys.* **123**, 204107 (2005).
- [11] V. Averbukh and L. S. Cederbaum, *J. Chem. Phys.* **125**, 094107 (2006).
- [12] R. Santra and L. S. Cederbaum, *Phys. Rev. Lett.* **90**, 153401 (2003).
- [13] S. Marburger, O. Kugeler, U. Hergenhahn, and T. Möller, *Phys. Rev. Lett.* **90**, 203401 (2003).
- [14] T. Jahnke *et al.*, *Phys. Rev. Lett.* **93**, 163401 (2004).
- [15] G. Öhrwall *et al.*, *Phys. Rev. Lett.* **93**, 173401 (2004).
- [16] V. Averbukh, I. B. Müller, and L. S. Cederbaum, *Phys. Rev. Lett.* **93**, 263002 (2004).
- [17] Y. Morishita *et al.*, *Phys. Rev. Lett.* **96**, 243402 (2006).
- [18] T. Jahnke *et al.*, *Nat. Phys.* **6**, 139 (2010).
- [19] M. Mucke, M. Braune, S. Barth, M. Förstel, T. Lischke, V. Ulrich, T. Arion, U. Becker, A. Bradshaw, and U. Hergenhahn, *Nat. Phys.* **6**, 143 (2010).
- [20] C. Buth, R. Santra, and L. S. Cederbaum, *J. Chem. Phys.* **119**, 10575 (2003).
- [21] E. F. Aziz, N. Ottosson, M. Faubel, I. V. Hertel, and B. Winter, *Nature (London)* **455**, 89 (2008).
- [22] W. Pokapanich *et al.*, *J. Am. Chem. Soc.* **131**, 7264 (2009).
- [23] N. Sisourat, N. V. Kryzhevoi, P. Kolorenč, S. Scheit, T. Jahnke, and L. S. Cederbaum, *Nat. Phys.* **6**, 508 (2010).
- [24] M. W. Schmidt *et al.*, *J. Comput. Chem.* **14**, 1347 (1993).
- [25] T. van Mourik, A. K. Wilson, and T. H. Dunning Jr., *Mol. Phys.* **96**, 529 (1999).
- [26] K. Kaufmann, W. Baumeister, and M. Jungen, *J. Phys. B* **22**, 2223 (1989).
- [27] G. Karlström *et al.*, *Comput. Mater. Sci.* **28**, 222 (2003).
- [28] L. Pauling, *J. Chem. Phys.* **1**, 56 (1933).
- [29] H. Yagisawa, H. Sato, and T. Watanabe, *Phys. Rev. A* **16**, 1352 (1977).
- [30] A. Metropoulo and C. A. Nicolaides, *Chem. Phys.* **114**, 1 (1987).
- [31] A. Belkacem, E. P. Kanter, R. E. Mitchell, Z. Vager, and B. J. Zabransky, *Phys. Rev. Lett.* **63**, 2555 (1989).
- [32] G. W. F. Drake, J. Kwela, and A. van Wijngaarden, *Phys. Rev. A* **46**, 113 (1992).
- [33] M. H. Prior, *Phys. Rev. Lett.* **29**, 611 (1972).
- [34] R. Santra and L. S. Cederbaum, *Phys. Rep.* **368**, 1 (2002).
- [35] K. Gokhberg, S. Kopelke, N. V. Kryzhevoi, P. Kolorenč, and L. S. Cederbaum, *Phys. Rev. A* **81**, 013417 (2010).
- [36] R. Santra, J. Zobeley, and L. S. Cederbaum, *Phys. Rev. B* **64**, 245104 (2001).